The Company of **Biologists**

RESEARCH ARTICLE

Arg tyrosine kinase modulates TGF-β1 production in human renal tubular cells under high-glucose conditions

Barbara Torsello[1],*, Cristina Bianchi[1],*, Chiara Meregalli[1], Vitalba Di Stefano[1], Lara Invernizzi[1], Sofia De Marco[1], Giorgio Bovo[2], Rinaldo Brivio[3], Guido Strada[4], Silvia Bombelli[1] and Roberto A. Perego[1],‡

ABSTRACT

Renal tubular cells are involved in the tubular interstitial fibrosis observed in diabetic nephropathy. It is debated whether epithelial–mesenchymal transition (EMT) affects tubular cells, which under high-glucose conditions overproduce transforming growth factor-β (TGF-β), a fibrogenic cytokine involved in interstitial fibrosis development. Our study investigated the involvement of non-receptor tyrosine kinase Arg (also called Abl2) in TGF-β production. Human primary tubular cell cultures exposed to high-glucose conditions were used. These cells showed an elongated morphology, stress fibers and vimentin increment but maintained most of the epithelial marker expression and distribution. In these cells exposed to high glucose, which overexpressed and secreted active TGF-β1, Arg protein and activity was downregulated. A further TGF-β1 increase was induced by Arg silencing with siRNA, as with the Arg tyrosine kinase inhibitor Imatinib. In the cells exposed to high glucose, reactive oxygen species (ROS)-dependent Arg kinase downregulation induced both RhoA activation, through p190RhoGAPA (also known as ARHGAP35) modulation, and proteasome activity inhibition. These data evidence a new specific involvement of Arg kinase into the regulation of TGF-β1 expression in tubular cells under high-glucose conditions and provide cues for new translational approaches in diabetic nephropathy.

INTRODUCTION

Diabetic nephropathy is a complication occurring in ∼35% of patients affected by diabetes mellitus and is the leading cause of end-stage renal disease in the developed world (de Boer et al., 2011). Chronic exposure to elevated blood glucose concentration contributes to the tubulointerstitial changes observed in overt diabetic nephropathy, characterized by thickening of tubular basement membrane, tubular atrophy and interstitial fibrosis (Gilbert and Cooper, 1999). These changes suggest a tubular cell involvement in diabetic nephropathy establishment. However, what is the main cellular type responsible for extracellular matrix deposition is still a matter of debate. Some studies have shown that tubular cells might undergo an *in vitro* epithelial–mesenchymal transition (EMT) and have a direct role in

tubulointerstitial fibrosis development (Lee and Han, 2010; Hills et al., 2012; Gu et al., 2013). However, conclusive evidence of a full EMT process *in vivo* is a controversial point. In fact, some papers provide evidence *in vivo* of human and rodent tubular cell EMT as a source of matrix-producing interstitial fibroblasts (Iwano et al., 2002; Rastaldi et al., 2002; Burns et al., 2006), and of mouse tubular cells producing collagen without evidence of EMT (Koesters et al., 2010; Fragiadaki et al., 2011). Instead, other *in vivo* models show that interstitial pericytes and resident fibroblasts, but not tubular cells, might be myofibroblast progenitors (Lin et al., 2008; Humphreys et al., 2010). Nevertheless, the involvement of tubular cells in interstitial fibrosis is also suggested by the finding that under high-glucose conditions (hereafter high-glucose-treated) human HK-2 and mouse MCT proximal tubular cell lines increase their *in vitro* production of TGF-β (Rocco et al., 1992; Fraser et al., 2003), one of the most important fibrogenic cytokines involved in development of renal interstitial fibrosis (Shen et al., 2013).

Of note, a role in downregulation of TGF-β signaling, through inhibition of c-Abl (also known as Abl1) and PDGFRβ activity in fibroblasts of animal models of renal and lung fibrosis (Daniels et al., 2004; Wang et al., 2005, 2010), has been described for Imatinib, an inhibitor of c-Abl, Arg (also known as Abl2), c-Kit and PDGFRβ tyrosine kinase activity (Buchdunger et al., 1996; Druker and Lydon, 2000; Okuda et al., 2001). Interestingly, there is also evidence that treatment with proteasome inhibitors prevents lung, skin and kidney fibrosis in different animal models (Tashiro et al., 2003; Luo et al., 2011; Mutlu et al., 2012). In fact, the ubiquitin–proteasome system, in addition to its role in protein turnover, plays a modulation role in many cellular signaling pathways, including those involving TGF-β1 (Elliott et al., 2003; Mutlu et al., 2012). Remarkably, it has been described that c-Abl and Arg tyrosine kinases associate with and phosphorylate the proteasome PSMA7 subunit with consequent inhibition of proteasome activity (Liu et al., 2006). Arg is also involved in some aspects of the EMT process, like cell migration and cytoskeleton modulation through the RhoA–ROCK pathway (Hernández et al., 2004; Peacock et al., 2007; Bianchi et al., 2013), which is also involved in TGF-β secretion in a high-glucose-treated HK-2 cell line (Gu et al., 2013). Based on these data, in the current study we analyzed the involvement of Arg tyrosine kinase in the production of TGF-β1 induced in well-characterized human primary tubular cell cultures (Perego et al., 2005; Bianchi et al., 2010; Cifola et al., 2011) by treatment with high glucose, which also induced some phenotypical and molecular changes in these tubular cells.

RESULTS

Phenotypical characterization of high-glucose-treated primary tubular cell cultures

We assessed whether high-glucose treatment could induce phenotypical changes in renal tubular primary cells cultured for

[1]School of Medicine and Surgery, Milano-Bicocca University, Monza 20900, Italy.
[2]Anatomo-Pathology Unit, San Gerardo Hospital, Monza 20900, Italy. [3]Clinical Pathology Unit, San Gerardo Hospital, Monza 20900, Italy. [4]Urology Unit, Bassini ICP Hospital, Milano 20092, Italy.
*These authors contributed equally to this work and both must be considered as first authors

‡Author for correspondence (roberto.perego@unimib.it)

C.B., 0000-0001-6305-1487; R.A.P., 0000-0003-3053-3476

Journal of Cell Science

7 days with high-glucose medium. In phase-contrast microscopy images, we observed that high-glucose-treated cells appeared more elongated with respect to the cobblestone morphology of control cells (Fig. 1A), as confirmed by the distribution of immunofluorescence signal for the epithelial markers cytokeratin and Epcam, which were maintained in treated cells (Fig. 1B; Fig. S1A). The epithelial proximal tubular marker N-cadherin and distal tubular marker E-cadherin maintained a membrane distribution and did not colocalize, even in high-glucose-treated cells (Fig. 1C). Proximal tubular markers CD13 (also known as ANPEP) and AQP1 were detected only in N-cadherin- and not in E-cadherin-positive cells, and distal tubular marker calbindin was detected only in E-cadherin- but not in N-cadherin-positive cells, in both treated and control cells (Fig. 1D,E; Fig. S1B). These data confirmed the mutually exclusive expression of N- and E-cadherin in proximal and distal tubular cells, respectively, as described previously (Bombelli et al., 2013), and here also shown under high-glucose conditions. Thus, tubular primary cells cultured in high-glucose medium changed the morphology but maintained the cellular distribution of epithelial markers as in control cells. No differences in cell viability between control and high-glucose-treated cells were observed (Fig. S2A).

Analysis of markers related to EMT after high-glucose treatment

We evaluated in our tubular cell cultures the effect of high-glucose treatment on the expression of markers involved in the EMT process, as characterized by downregulation of epithelial markers and upregulation of mesenchymal markers (Carew et al., 2012). As shown by real-time quantitative PCR (Fig. 2A), the transcript level of the epithelial markers N- and E-cadherin, the mesenchymal markers Col1a2 and S100A4, and miR-200c, an indirect inducer of E-cadherin expression, did not significantly change during high-glucose treatment. At the protein level (Fig. 2B), the epithelial marker ZO-1 (also known as TJP1) and the epithelial proximal tubular marker N-cadherin were downregulated after 7 days and 96 h of high-glucose treatment, respectively. Instead, E-cadherin maintained a similar expression level both in control and treated cells. The mesenchymal marker vimentin was upregulated after 7 days of high-glucose treatment, but α-smooth muscle actin (α-sma) expression was not induced by the treatment. Moreover, the treatment with high glucose did not significantly change the percentage of proximal (CD13 positive) tubular cells in our primary cell cultures (Fig. S1C) and the protein expression level of the proximal (AQP1) and distal (calbindin) tubular markers also did not change, even at 7 days of treatment (Fig. S1D). Thus, in high-glucose-treated cultures, EMT markers were only partially modulated and the changes observed were not the effect of the outgrowth of a specific tubular cell population on the other population.

Stress fiber density and cell migration analysis after high-glucose treatment

Given that the acquisition of prominent cytoplasmic stress fibers is an EMT feature correlated with cell motility (Liu, 2004), we analyzed these two characteristics in tubular cells cultured in high-glucose medium. We observed that these cells had F-actin organized in dense stress fibers across the cytoplasm, whereas control tubular cells had a cortical localization of F-actin with rarer and thinner cytoplasmic stress fibers. The increase of cytoplasmic stress fiber density was significant after 96 h of high-glucose treatment (Fig. 3A). Moreover, as assessed by a wound healing assay, cells treated with high-glucose for 96 h had a wound recovery significantly lower than control ones after 8 h from the 'scratch' (Fig. 3B). Treated cells also evidenced a cell motility reduction as
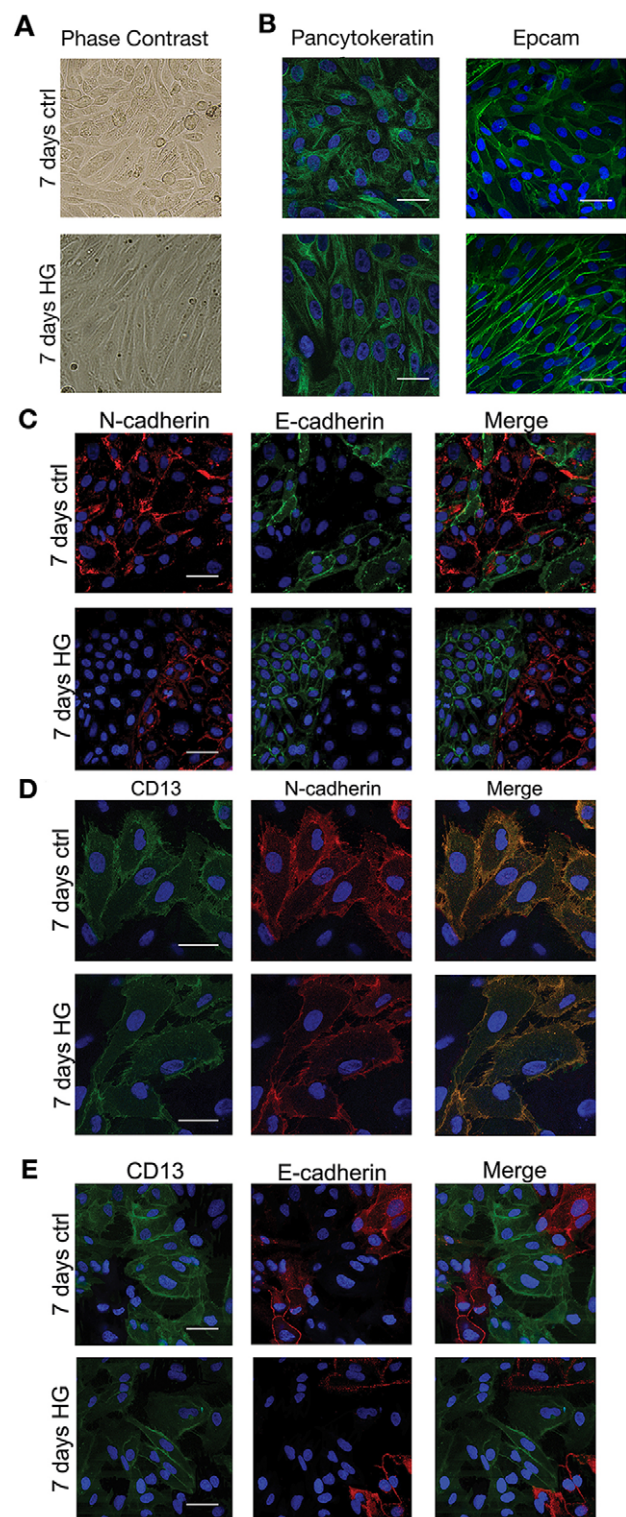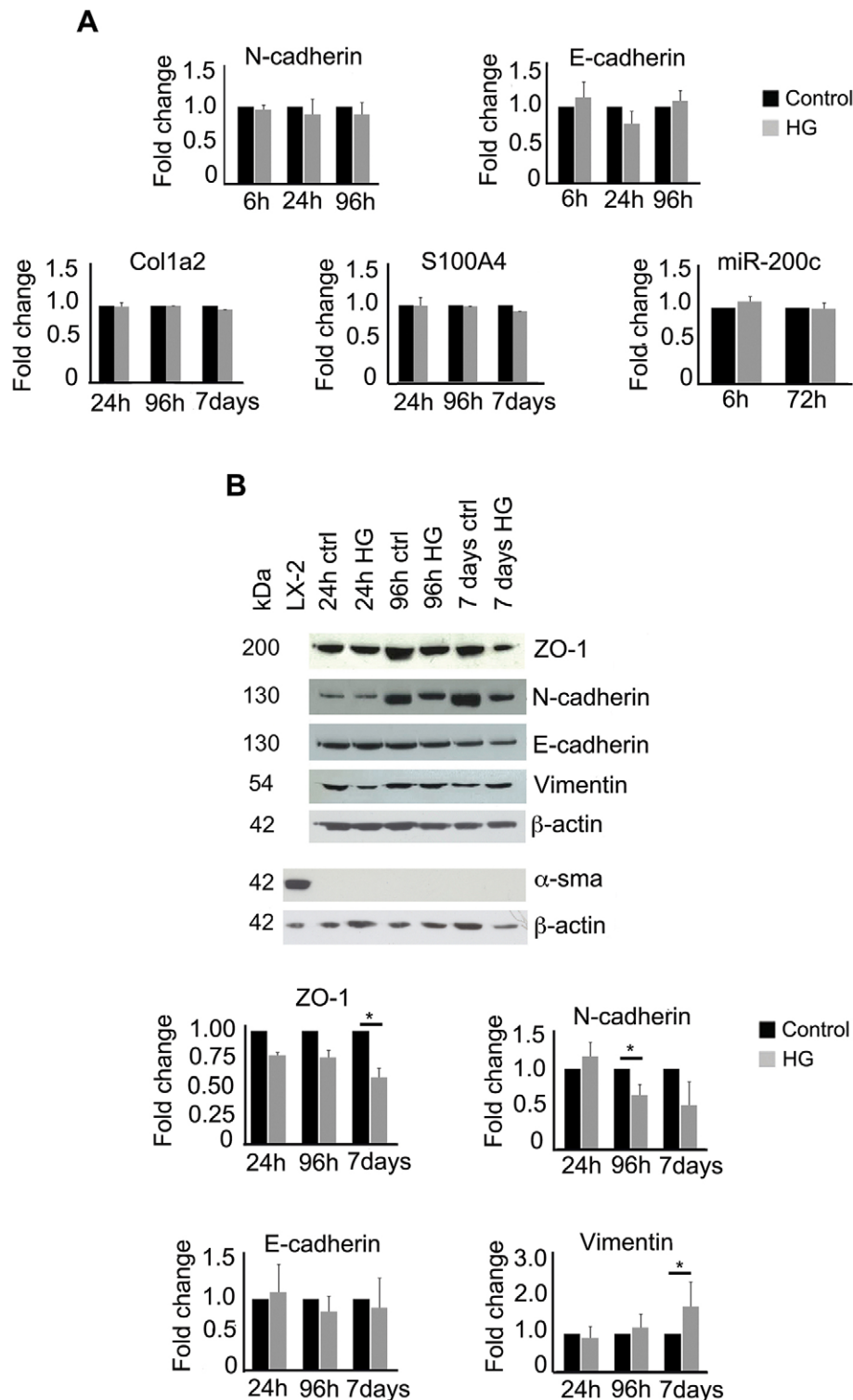

Fig. 1. Morphological evaluation and cellular distribution of renal proximal and distal epithelial tubular markers. Representative images of primary cell cultures treated for 7 days with control (ctrl) or high glucose (HG) medium. (A) Phase-contrast images showing morphological differences (200x). (B–E) Confocal microscopy images of (B) the epithelial markers pancytokeratin and Epcam (green), (C) the epithelial proximal tubular marker N-cadherin (red) and distal tubular marker E-cadherin (green), which did not colocalize (merge); (D) proximal tubular markers CD13 (green) and N-cadherin (red), which colocalize in control and high-glucose-treated cells (merge); and (E) CD13 (green) and E-cadherin (red), which did not colocalize (merge). DAPI was used to counterstain the nuclei in blue. Scale bars: 10 μm.

Fig. 2. Expression of EMT markers in control and high-glucose-treated primary tubular cell cultures. (A) N-cadherin, E-cadherin, Col1a2, S100A4 transcript and miRNA 200c levels were evaluated by real-time PCR at different time points in control (ctrl) and high-glucose (HG) conditions. The relative amounts of the different transcripts, calculated as $2^{-\Delta\Delta Ct}$, are represented as fold change with respect to the corresponding control sample (unpaired t-test, $n=4$, mean±s.d.). (B) Western blots of cellular protein lysates of representative experiments showing the bands of indicated markers and corresponding β-actin level at different time points. The normalized band intensities of specific proteins are expressed as a fold change with respect to corresponding control samples (unpaired t-test, *$P<0.05$, $n=7$, mean±s.d.) LX-2, LX-2 human fibroblast cell line lysate used as α-sma positive control.

assessed by a Boyden chamber assay (Fig. S2B). Thus, the cytoskeletal changes of high-glucose-treated tubular cells were consistent with EMT features but their functional behavior was not.

In primary tubular cell cultures high-glucose treatment induced an increase of TGF-β1 expression and secretion that activated fibroblasts

In our tubular primary cultures, we observed a significant upregulation of TGF-β1 transcript and precursor protein at 72 and 96 h of high-glucose treatment, respectively (Fig. 4A,B). An increased secretion of TGF-β1 was also evident in the medium of tubular cells treated with high glucose for 96 h (Fig. 4C). NIH3T3 fibroblasts grew significantly faster when cultured in conditioned medium of high-glucose-treated tubular cells (high-glucose conditioned medium) compared to those grown in non-conditioned fibroblast medium, in control cell conditioned medium and in high-glucose conditioned medium plus TGF-β receptor inhibitor SB431542 (Fig. 4D). In addition, the expression
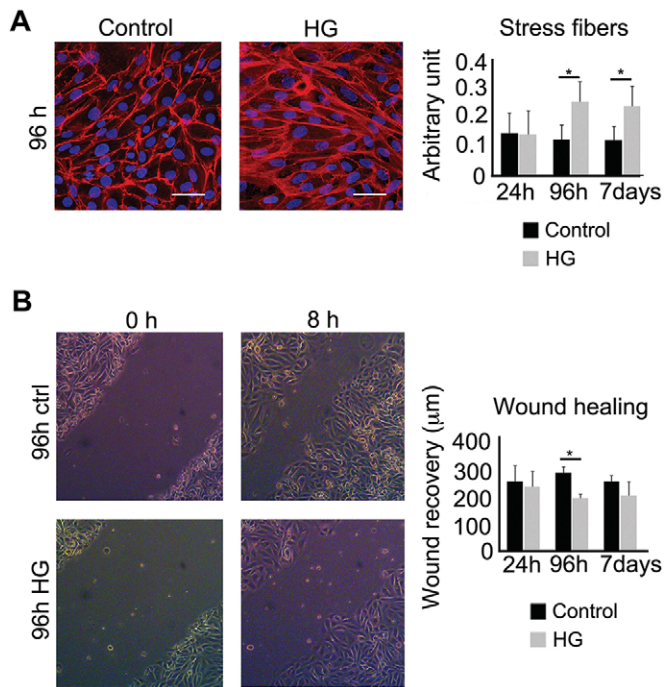
Fig. 3. High-glucose treatment increases stress fiber density but decreases cell migration of primary tubular cell cultures.
(A) Representative images of 96 h control (ctrl) and high-glucose (HG)-treated primary cultures stained with Alexa-Fluor-594–phalloidin (red) and counterstained with DAPI (blue), and analyzed by confocal microscopy; stress fiber density quantification is expressed in the graph as arbitrary units (unpaired t-test, *$P<0.05$, $n=3$, a minimum of 50 cells was analyzed per sample, mean±s.d.). (B) Representative images of the wound healing assay after the scratch (0 h) and after 8 h (8 h) of wound recovering performed on 96 h control (ctrl) and high-glucose (HG)-treated primary cultures; the graph indicates the wound recovery calculated in µm as difference between initial and final wound width (unpaired t-test, *$P<0.05$, $n=4$, mean±s.d.).

of α-sma protein, a cytoskeletal marker in activated fibroblasts, and the level of phosphorylated Smad2 protein, a specific target of the activated TGF-β pathway (Hills and Squires, 2011), significantly increased only in NIH3T3 cells treated with high-glucose conditioned medium. However, α-sma and phosphorylated Smad2 protein expression was strongly downregulated when SB431542 was present in high-glucose conditioned medium (Fig. 4E,F). These data show that primary tubular cell cultures under high-glucose conditions overexpressed and secreted active TGF-β1 that induced fibroblast activation.

Imatinib induced a further increase of TGF-β1 expression and secretion in high-glucose-treated tubular cells
To evaluate how TGF-β1 production was modulated in our cellular model, we tested the response of tubular cells to Imatinib treatment. It has been demonstrated that 10 µM Imatinib prevents TGF-β-driven renal fibroblast activation *in vitro* (Wang et al., 2005), but when directly delivered *in vivo* to proximal tubular cells, Imatinib does not show anti-fibrotic efficacy (Dolman et al., 2012). Surprisingly, the treatment of our tubular cells with 10 µM Imatinib induced, only under high-glucose conditions, a further significant increment of TGF-β1 transcript, protein precursor and secretion (Fig. 5A–C) without changes in cell viability (Fig. S2A). Moreover, the expression of α-sma protein and the level of phosphorylated Smad2 protein significantly increased in NIH3T3 cells grown in the presence of high-glucose plus Imatinib

conditioned medium with respect to high-glucose conditioned medium (Fig. 5D,E). Even in this case, α-sma and phosphorylated Smad2 protein expression was strongly downregulated in high-glucose plus Imatinib conditioned medium in the presence of SB431542 (Fig. 5D,E). Thus, in tubular cells under high-glucose conditions Imatinib induced a further upregulation of TGF-β1 production that further activated fibroblasts.

High-glucose treatment downregulated Arg protein in tubular cells
To gain further insight into the molecular mechanism involved in TGF-β1 production, we tested the well-known targets of Imatinib inhibitory activity (Buchdunger et al., 1996; Druker and Lydon, 2000; Okuda et al., 2001). PDGFRβ and c-Kit were not expressed in our control and treated cells, and the c-Abl protein level did not change with high-glucose treatment (Fig. S2C,D). Instead, Arg protein was significantly downregulated at 96 h of high-glucose treatment (Fig. 6A), but it did not decrease in control and high-glucose-treated tubular cells grown in the presence of Imatinib (Fig. 6B). Thus, in primary tubular cell cultures, high-glucose treatment induced a downregulation of Arg protein that correlated with the increment of TGF-β1 expression and secretion observed in the same culture condition (Fig. 4A–C).

High glucose induced an increase in ubiquitin-dependent Arg degradation in tubular cells through a ROS level increment
It has been described that the MCF-7 and 293 cell line exposure to reactive oxygen species (ROS) induced an increase of Arg ubiquitylation and degradation (Cao et al., 2005), and that high-glucose conditions induced ROS overload in tubular cells (Lee et al., 2013). To evaluate whether these molecular mechanisms were even active in our *in vitro* model, we assayed ROS production in tubular cells and found that high-glucose treatment for 96 h induced a significant increment of ROS level that further increased at 7 days (Fig. 6C). Under high-glucose conditions the Arg transcript level did not change (data not shown), but Arg protein ubiquitylation increased (Fig. 6D), with consequent degradation by the proteasome that could be counteracted by the proteasome inhibitor MG132 (Fig. S3A,B). Moreover, the addition of the antioxidant NAC in high-glucose medium, which significantly decreased ROS production (Fig. 6C), reversed high-glucose-induced downregulation of Arg protein (Fig. 6E), confirming that, in our model, high-glucose-induced ROS were responsible for the decrease in Arg protein. Notably, high levels of endogenous ROS persisted even when Imatinib was present in high-glucose medium (Fig. 6C), but in this case Arg protein ubiquitylation did not increase with respect to control (Fig. 6D). In addition, we excluded that the observed downregulation of Arg was related to a decrease in N-cadherin. In fact, the knockdown of N-cadherin by siRNA in tubular cells grown in control medium did not affect Arg expression (Fig. S3C). Thus, oxidative stress induced by high-glucose treatment was responsible for the Arg ubiquitylation and degradation.

High-glucose induced TGF-β1 upregulation, proteasome inhibition and RhoA activation through Arg activity downregulation in tubular cells
To prove the specific involvement of Arg in the TGF-β1 upregulation, we evaluated TGF-β1 expression and secretion after Arg silencing by small interfering RNA (siRNA). Arg knockdown (Fig. S3D) further improved TGF-β1 expression and secretion in high-glucose-treated cells at 96 h (Fig. 7A,B), mimicking the
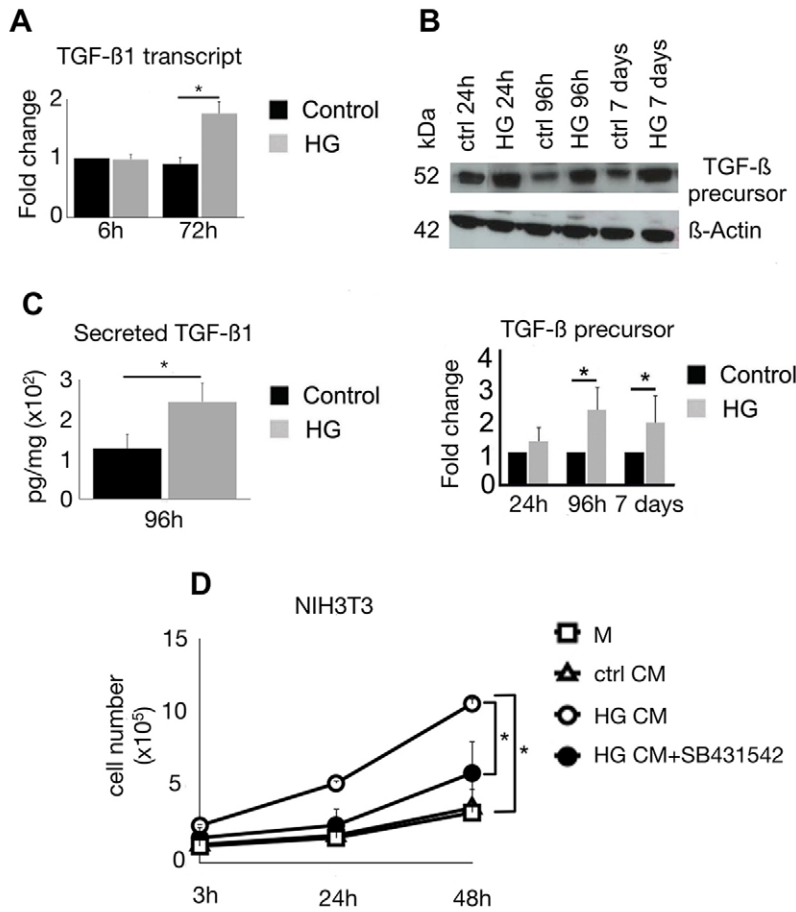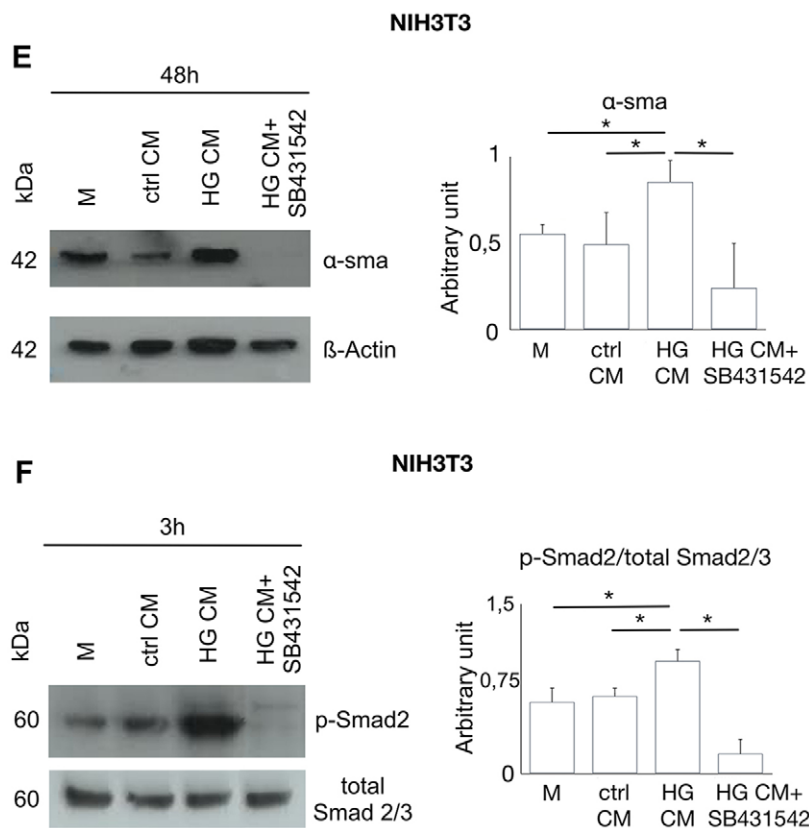
Fig. 4. High glucose induces an increase in TGF-β expression and secretion in tubular cells that activates NIH3T3 fibroblasts. (A) Real-time PCR of TGF-β1 transcript in tubular cell cultures after 6 and 72 h of high-glucose (HG) treatment. The relative amounts are represented as fold change with respect to corresponding control (unpaired *t*-test, *$P<0.05$, $n=3$, mean±s.d.). (B) Representative western blot of lysates from tubular cells cultured for different time points in control (ctrl) or in high-glucose (HG) medium. The protein bands for the TGF-β precursor and for β-actin are shown. In the graph, the normalized TGF-β band intensities are expressed as fold change with respect to corresponding control sample (unpaired *t*-test, *$P<0.05$, $n=5$, mean±s.d.). (C) ELISA for secreted TGF-β1 in conditioned medium of tubular cells cultured for 96 h in control or in high-glucose medium (unpaired *t*-test, *$P<0.05$, $n=4$, mean±s.d.). (D) Growth curves of NIH3T3 fibroblasts cultured in fibroblast medium (white squares, M), in control conditioned medium (white triangles, ctrl CM), in high-glucose conditioned medium (white circles, HG CM) or in high-glucose conditioned medium with SB431542 (black circles, HG CM+SB431542) (one-way ANOVA with Bonferroni's test, *$P<0.05$, $n=3$, mean±s.d.). (E,F) Representative western blots of protein lysates of NIH3T3 fibroblasts, cultured for 3 or 48 h in the indicated medium. The protein bands of (E) α-sma and β-Actin and (F) phospho-Smad2 (p-Smad2) and total Smad (total Smad2/3) and corresponding quantification graph of normalized bands are shown. Phosho-Smad2 (p-Smad2) was normalized to the corresponding total Smad 2/3 (one-way ANOVA with Bonferroni's test, *$P<0.05$, $n=3$, mean±s.d.).
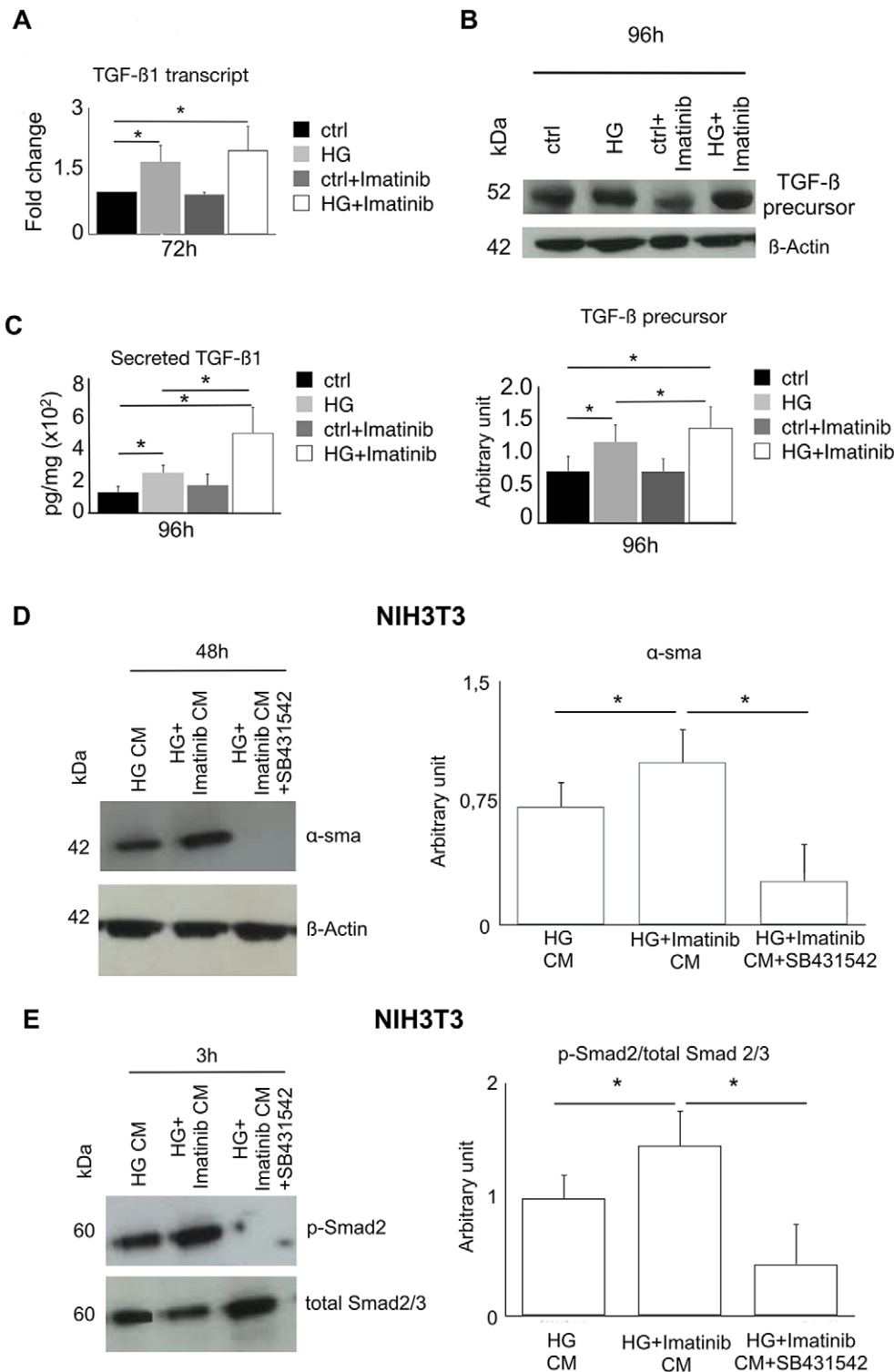
Fig. 5. Imatinib induces a further increase of TGF-β1 expression and secretion in high-glucose-treated primary tubular cell cultures that further activates NIH3T3 fibroblasts. (A) Real-time PCR of TGF-β1 transcript in tubular cells cultured for 72 h in control (ctrl) medium, in high-glucose medium (HG), in control medium plus Imatinib (ctrl+Imatinib) or high-glucose medium plus Imatinib (HG+Imatinib). The relative amounts are represented as the fold change with respect to the control sample (one-way ANOVA with Bonferroni's test, *$P<0.05$, $n=3$, mean±s.d.). (B) Representative western blot of lysates from tubular cells cultured for 96 h in the indicated medium. The protein bands of the TGF-β precursor and of β-actin are shown. In the graph, the normalized TGF-β band intensities are reported (one-way ANOVA with Bonferroni's test, *$P<0.05$, $n=5$). (C) ELISA for secreted TGF-β1 in conditioned medium of tubular cells cultured for 96 h in the indicated medium (one-way ANOVA with Bonferroni's test, *$P<0.05$, $n=4$, mean±s.d.). (D,E) Representative western blots of protein lysates of NIH3T3 fibroblasts, cultured for 3 or 48 h in high-glucose conditioned medium (HG CM), in high-glucose plus Imatinib conditioned medium (HG+Imatinib CM) or in high-glucose plus Imatinib conditioned medium with SB431542 (HG+Imatinib CM+SB431542). The protein bands of (D) α-sma and β-actin and (E) phospho-Smad2 (p-Smad2) and total Smad (total Smad 2/3) and the corresponding quantification graph of normalized bands are shown. Phospho-Smad2 (p-Smad2) was normalized for corresponding total Smad 2/3 (one-way ANOVA with Bonferroni's test, *$P<0.05$, $n=3$, mean±s.d.).

Imatinib effect (Fig. 5B,C), and showing that Arg is specifically involved in the TGF-β1 upregulation in high-glucose-treated tubular cells.

To study in depth the Arg-dependent modulation of TGF-β1 production, we investigated both the proteasome activity and Rho-ROCK signaling. As expected (Tashiro et al., 2003; Mutlu et al., 2012), specific proteasome inhibition by MG132 induced a significant downregulation of TGF-β in high-glucose-treated cells (Fig. S3A,E). However, in our high-glucose-treated cells, TGF-β1

increased (Fig. 5A–C) even though the proteasome activity was downregulated (Fig. S3F). Moreover, in these cells Arg activity also decreased as proved by the decrease of tyrosine-phosphorylated Arg and site-specific (Y1105) phosphorylated p190RhoGAPA protein (also known as ARHGAP35), a well-known Arg kinase specific target and RhoA inhibitor (Hernández et al., 2004) (Fig. S3G,H). In high-glucose-treated cells Arg knockdown with siRNA induced a further proteasome inhibition, in spite of a further TGF-β1 increase (Fig. 7A–C). The treatment of tubular cells with high glucose plus
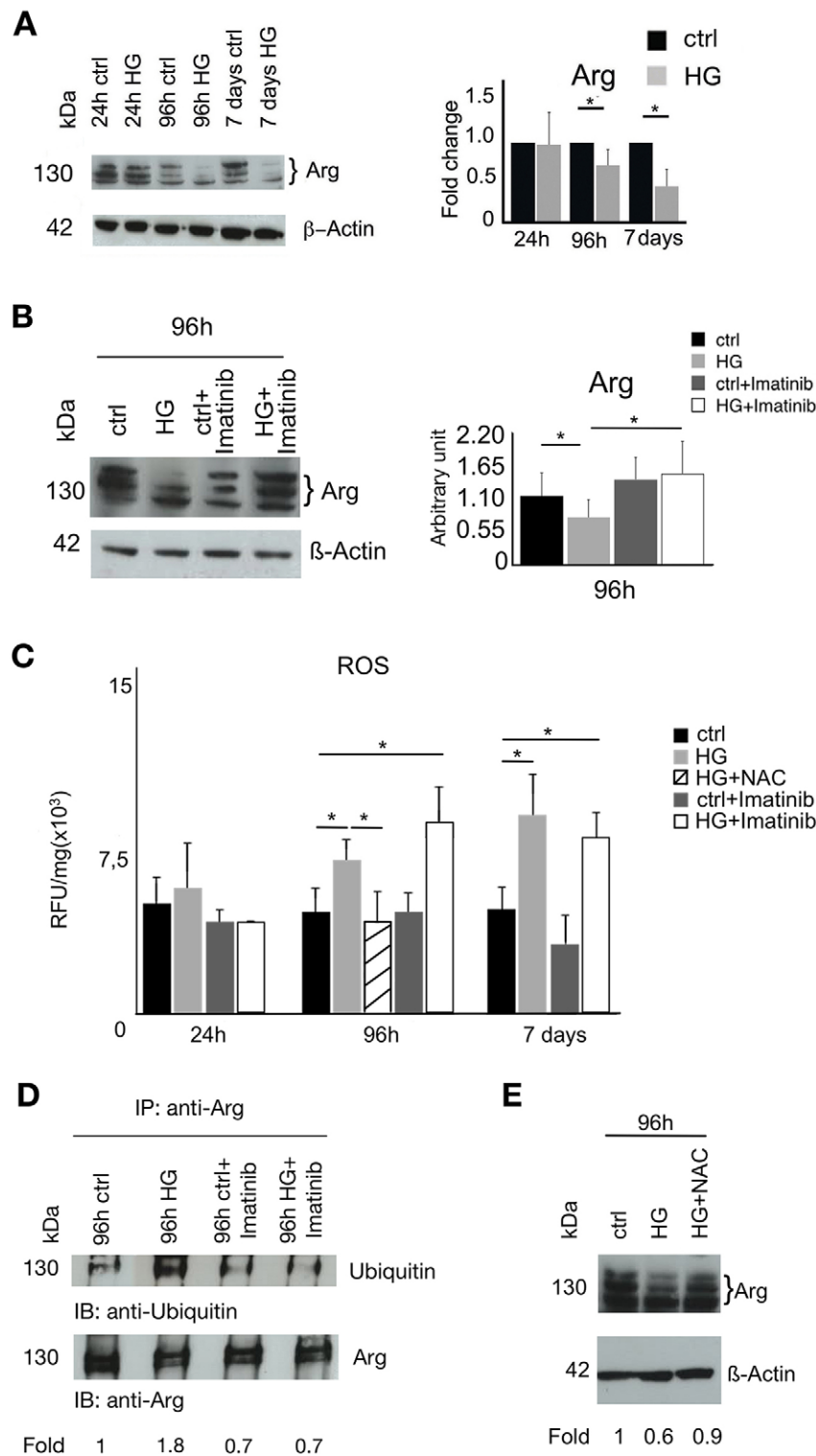
Fig. 6. High glucose induces downregulation of Arg protein through ROS level increase.
(A,B) Representative western blot of protein lysates obtained from tubular cells cultured for indicated time points in control (ctrl) medium, in high-glucose medium (HG), control medium plus Imatinib (ctrl+Imatinib) or high-glucose medium plus Imatinib (HG+Imatinib). Arg and β-actin protein bands are shown. The normalized Arg band intensities are expressed in A as the fold change with respect to corresponding control samples (unpaired t-test, *$P<0.05$, $n=7$, mean±s.d.), and in B as arbitrary units (one-way ANOVA with Bonferroni's test, *$P<0.05$, $n=4$, mean± s.d.). (C) Cell homogenates obtained from tubular cultures grown for indicated time points in control (ctrl), high-glucose (HG), high-glucose plus NAC (HG+NAC), control plus Imatinib (crtl+Imatinib) or high-glucose plus Imatinib (HG+Imatinib) medium and assayed for fluorescent oxidized DCF content. The mean±s.d. of relative fluorescence normalized to the cell protein concentration (RFU/mg) is shown (one-way ANOVA with Bonferroni's test, *$P<0.05$, $n=5$). (D) Cellular protein lysates of primary cultures, grown for 96 h in the indicated medium, immunoprecipitated with anti-Arg antibodies, blotted and hybridized with anti-ubiquitin and anti-Arg antibodies. The ubiquitin band intensities normalized to the corresponding Arg band intensities are expressed as the fold change with respect to the control sample. (E) Representative western blot of tubular cells cultured for 96 h in control, high-glucose or high-glucose+NAC medium. Arg protein band intensities normalized to the corresponding β-actin band are expressed as fold change with respect to the control sample.

Imatinib, which inhibited Arg kinase activity (Fig. S3G,H), upregulated TGF-β1 but did not affect the proteasome (Fig. 5A–C; Fig. S3F). Thus, TGF-β1 overproduction induced in our cellular model by Arg tyrosine kinase downregulation did not seem to be mediated by an Arg-dependent inhibition of proteasome activity.

Next, we evaluated whether Arg downregulation could induce TGF-β1 overproduction through the activation of RhoA-ROCK signaling. The amount of phospho-Y1105-p190RhoGAPA protein decreased after 96 h of high-glucose treatment (Fig. 7D), as did the amount of Arg protein and its phosphorylated form (Fig. 6A; Fig. S3G), and the amount of RhoA-GTP (the activated state of RhoA) increased (Fig. 7E,F). Arg knockdown by siRNA, which further increased TGF-β1 production in high-glucose-treated cells, noticeably decreased the level of phospho-Y1105-p190RhoGAPA protein (Fig. 7A,G). Thus, in our tubular cells treated with high-glucose, Arg kinase downregulation caused a decrease in p190RhoGAPA phosphorylation, the activation of RhoA and induced TGF-β1 upregulation.
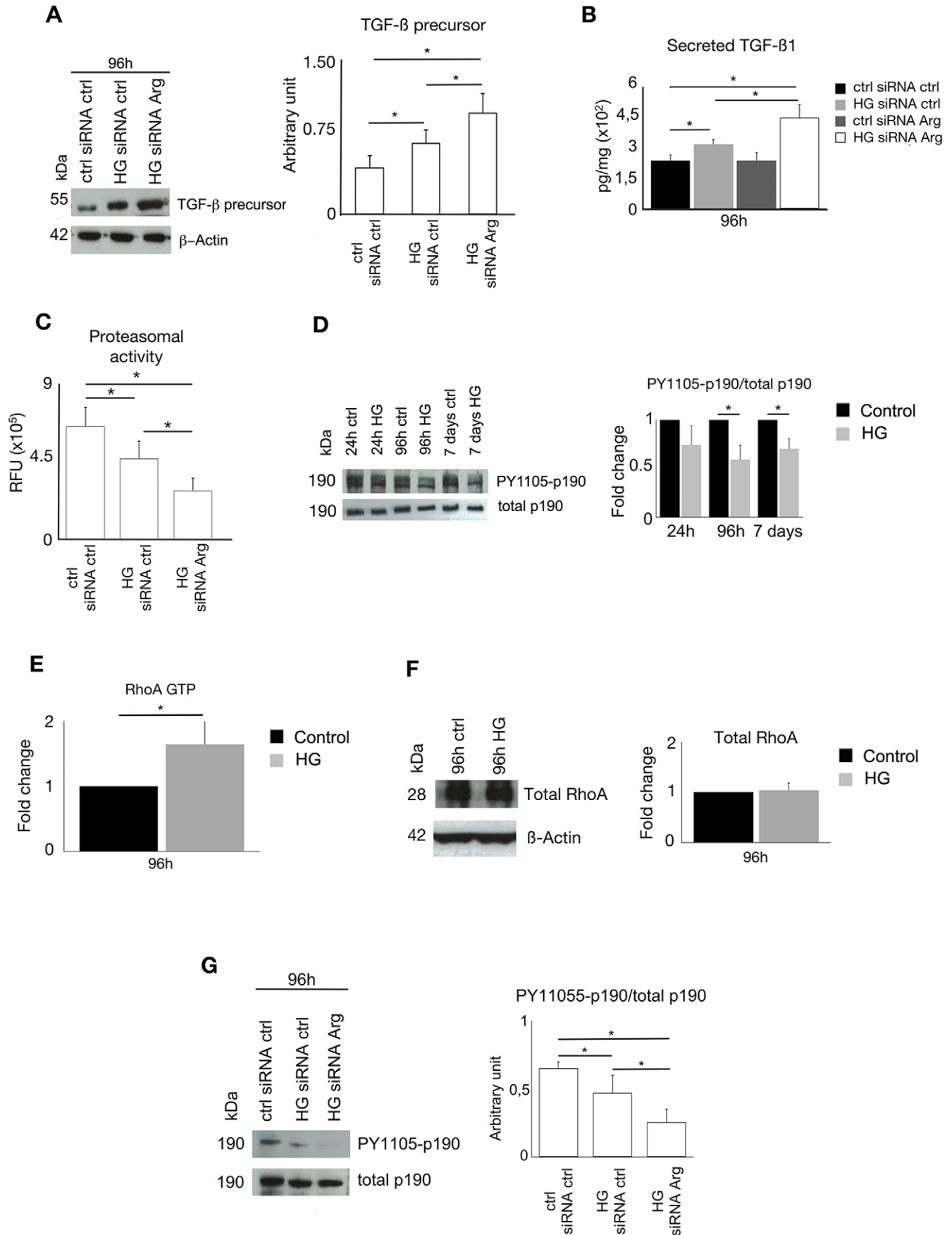
Fig. 7. See next page for legend.

Fig. 7. Arg silencing induces a further increase of TGF-β1 expression and secretion, proteasome inhibition and phospho-Y1105-p190RhoGAPA downregulation in high-glucose-treated tubular cells. (A,C,G) Protein lysates obtained from primary cultures grown for 96 h in control medium plus control siRNA (ctrl siRNA ctrl), high-glucose medium plus control siRNA (HG), or high-glucose medium plus Arg-specific siRNA (HG siRNA Arg), were assayed for (A) TGF-β precursor protein and (G) site-specific (Y1105) phosphorylated p190RhoGAPA (PY1105-p190) by western blotting, and (C) for proteasome activity by addition of Suc-LLVT-AMC substrate and quantification of the released fluorescent signal. Normalized TGF-β band intensities (A), mean relative fluorescent units (RFU) (C), and PY1105-p190 band intensities normalized to the corresponding total p190RhoGAPA (total p190) band (G) are reported in the graphs as mean±s.d. (one-way ANOVA with Bonferroni's test, *P<0.05, n=4). (B) ELISA for secreted TGF-β1 in conditioned medium of tubular cells cultured for 96 h in indicated medium (one-way ANOVA with Bonferroni's test, *P<0.05, n=3, mean±s.d.). (D) Representative western blot of protein lysates from primary cultures grown for different time points in control (ctrl) or high-glucose (HG) media, showing the bands of PY1105-p190 and total p190RhoGAPA proteins. The PY1105-p190 band intensities were normalized to the corresponding total p190RhoGAPA band and expressed as fold change with respect to corresponding control samples (unpaired t-test, *P<0.05, n=3, mean±s.d.). (E,F) Protein lysates obtained from tubular cells grown for 96 h in control or high-glucose medium were assayed for (E) RhoA GTP level by G-LISA and (F) total RhoA protein by western blotting. RhoA-GTP (E) and normalized total RhoA (F) values are expressed as the fold change with respect to the control sample (unpaired t-test, *P<0.05, n=4, mean±s.d.). No difference in total RhoA level was seen after high-glucose treatment.

DISCUSSION

In order to undertake studies directed to understand the molecular and functional response of tubular cells to high-glucose conditions, we used human primary tubular cell cultures. These cultures represent a reproducible and well-characterized cellular model that maintains, in the first passages, the phenotypic and molecular characteristics of the corresponding tissue (Perego et al., 2005; Bianchi et al., 2010; Cifola et al., 2011). Our data showed that these primary cells, grown in high-glucose medium, acquired an elongated morphology but only a few molecular EMT features, and did not reach a full EMT phenotype. Thus, the phenotypical and functional features of our high-glucose-treated cells were more suggestive of an activated cellular state, which has also been described in other renal fibrosis models (Hertig et al., 2008), than an EMT. So far, little is known about the *in vitro* EMT susceptibility of human primary tubular cell cultures. Some reports suggest that human primary tubular cells, even after TGF-β treatment, the major factor driving EMT (Carew et al., 2012), show morphological alterations but maintain a stable expression of epithelial markers like E-cadherin and its indirect inducer miR-200c (Keller et al., 2012), as also seen in the results described here. Our high-glucose-treated primary cell cultures overexpressed and secreted TGF-β1 that was able to activate fibroblasts, and the TGF-β1 overexpression was associated with a significant decrease of Arg protein and activity. The further increase of TGF-β1 expression and secretion after Arg silencing confirmed this association. Therefore, Arg activity downregulation could be the key to the interpretation of TGF-β1 upregulation in our cellular model.

First of all we demonstrated that Arg-modulated TGF-β1 production was not mediated by an Arg-dependent inhibition of proteasome activity, as also confirmed by Arg silencing, which resulted in further proteasome inhibition and an increase in TGF-β1. Thus, in our experimental model, the proteasome and Arg activity decrease matched the increase in TGF-β1.

By contrast, in our cellular model Arg downregulation might induce upregulation of TGF-β1 through the activation of RhoA-ROCK signaling. In fact, in high-glucose-treated tubular cells, we

documented that Arg downregulation increased TGF-β1 production, decreased p190RhoGAPA specific phosphorylation and increased the RhoA-GTP level. Therefore, in our cellular model under high-glucose conditions, Arg kinase downregulation could activate the RhoA-ROCK signaling by reducing RhoA inhibition induced by p190RhoGAPA. The activation of this signaling would explain the increase of stress fibers (Hernández et al., 2004) and TGF-β1 production (Gu et al., 2013).

Of note, literature reports a reduction in the amount of TGF-β when the proteasome is directly inactivated by the specific inhibitor MG132 (Tashiro et al., 2003; Mutlu et al., 2012) and our data also confirmed this finding (Fig. S3A,E). The discrepancy between the effect induced on TGF-β expression by inhibition of proteasome activity with MG132 and Arg silencing, might be explained by the dual effects induced by Arg and c-Abl in our cells. In fact, in Arg-silenced cells the permanence of c-Abl might inhibit proteasome activity (Liu et al., 2006) with a consequent decrease in TGF-β . However, Arg deficiency might also induce an increase in TGF-β, through the decrease of p190RhoGAPA phosphorylation and consequent upregulation of RhoA-ROCK signaling (Gu et al., 2013).

Literature data also report a proteasome activation rather than reduction when Arg kinase activity is downregulated (Liu et al., 2006). However, a more recent paper (Li et al., 2015) shows that Arg and c-Abl, through the phosphorylation of proteasome subunit PSMA7, also induce an inhibition of proteasome degradation. Based on these new literature data, Arg silencing might result in a degradation of the proteasome that is unbalanced by an increase of its activity. This unbalance might explain the decrease of proteasome activity observed in Arg silenced cells.

We also demonstrated that the Arg kinase downregulation is determined by an increase of ROS. A high-glucose-dependent increase of ROS in tubular cells has been described as being caused by the overexpression of Nox4, the isoform of NADPH oxidase responsible for ROS production in several kidney diseases (Lee and Han, 2010; Lee et al., 2013). ROS promoted Arg degradation by ubiquitylation, whereas c-Abl seems to be less sensitive to high-glucose-induced ROS (Fig. S2D), as also described in other cellular models (Cao et al., 2005). The increase in ROS in the presence of high-glucose plus Imatinib did not induce an increase of Arg ubiquitylation and thus a decrease of Arg protein level because ROS induce Arg ubiquitylation when Arg is activated (Cao et al., 2005) and our data clearly showed that Arg activity was inhibited by Imatinib. High-glucose plus Imatinib did not affect proteasome activity probably because of opposite action of ROS, induced by high-glucose (Liu et al., 2006), and of c-Abl, a well-known proteasome inhibitor (Liu et al., 2006) inactivated by Imatinib.

A further significant increase of TGF-β1 in tubular cells was induced by high-glucose plus Imatinib treatment. Notably, in mouse models of diabetic nephropathy (Lassila et al., 2005) and immune-mediated kidney injury (Zoja et al., 2006), Imatinib has been described to reduce TGF-β1 expression in renal tissue, but the renal cell types and the molecular pathways targeted by Imatinib were not defined. In other animal models of renal fibrosis (Wang et al., 2005, 2010; Wallace and Gewin, 2013), Imatinib has been described to prevent TGF-β-dependent activation of fibroblasts. Interestingly, when directly delivered *in vivo* to proximal tubular cells in a mouse model of tubulointerstitial fibrosis, Imatinib did not show anti-fibrotic efficacy (Dolman et al., 2012) and this *in vivo* finding supports our *in vitro* data. Thus, the response to Imatinib seems to be cell type specific and influenced by microenvironment conditions, as suggested by our *in vitro* data that show that in Imatinib-treated

tubular cells there is TGF-β1 overexpression only under high-glucose conditions. Our *in vitro* cellular model highlights a specific response of high-glucose-treated tubular cells to Imatinib that might be hidden by the renal fibroblast response in *in vivo* models of diabetic nephropathy (Lassila et al., 2005). It is important to be aware of this specific response because, as proven in transgenic mice, the tubular TGF-β1 overexpression might be the cause of tubular autophagy and degeneration (Koesters et al., 2010).

In conclusion, the findings here describe evidence that Arg kinase downregulation is specifically involved in TGF-β1 upregulation and cytoskeleton alterations induced by high glucose in tubular cells. Our data could be useful in the development of new approaches to control TGF-β expression in tubular cells under diabetic conditions, and suggest that the response to Imatinib treatment is cell type specific, at least in kidneys of diabetic patients.

MATERIALS AND METHODS
Human primary tubular cell cultures and treatments
Normal renal cortex specimens were obtained from adult human kidneys surgically removed because of renal carcinoma, after written patients' informed consent and in accordance with recommendations of the Local Ethical Committee of Provincia Monza Brianza and the Declaration of Helsinki. Primary tubular cell cultures were obtained and characterized as previously described (Bianchi et al., 2010) from 30 different renal cortex tissue specimens. The cells, trypsinized at the first confluence, were diluted and re-plated to reach the second confluence at the end of each treatment point. In particular, after 24 h of serum starvation, the cells were cultured for up to 7 days in low-glucose Dulbecco's modified Eagle's medium (DMEM) (100 mg/dl glucose; control medium), or in high-glucose DMEM (450 mg/dl glucose; high-glucose medium), both supplemented with 10% fetal bovine serum (FBS), 1% glutamine, 1% penicillin-streptomycin and 1% amphotericin (Euroclone, Milan, Italy). The glucose concentration was regularly checked and restored to the appropriate level, when necessary, by addition of D-glucose (Sigma-Aldrich, St Louis, MO). Osmolarity balance was obtained by addition of D-mannitol (350 mg/dl; Sigma-Aldrich) to control medium. Specific tyrosine kinase activities and proteasome activity were, respectively, inhibited by addition of Imatinib mesylate (10 μM; Cayman Chemicals, Ann Arbor, MI) and MG132 (10 μM; Sigma-Aldrich) to control and high-glucose media. Antioxidative treatment was performed by addition of N-acetyl-L-cysteine (NAC) (10 mM; Sigma-Aldrich) to high-glucose medium.

Immunofluorescence and stress fiber analysis
Cells were seeded on glass coverslips, fixed and incubated with the indicated primary antibodies and, when necessary, with secondary antibodies (Table S1), as previously described (Bianchi et al., 2010). Stress fibers were labeled by Alexa-Fluor-594–phalloidin (dilution 1:100; Molecular Probes, Carlsberg, CA). Nuclei were counterstained with Mounting DAPI (Molecular Probes). Immunofluorescence pictures were obtained with confocal microscope Zeiss LSM710, using a 63× objective, equipped with Zen2009 software (Zeiss, Oberkochen, Germany). Stress fiber density quantification was obtained using NIH ImageJ software (http://www.rsbweb.nih.gor/iJ), as previously described (Bianchi et al., 2013).

RNA extraction and real-time quantitative PCR
Total RNA extraction and reverse transcription were carried out as previously described (Bianchi et al., 2008). Real-time quantitative PCR was carried out with a TaqMan Gene Expression Assay (Applied Biosystems, Foster City, CA) according to manufacturer's instructions, using commercial kits (Table S2). The amplifications were carried out in 20 μl reactions containing 50 ng of cDNA, 1× Universal PCR Master Mix, and corresponding primers and probes, in an ABI PRISM® 7900HT Fast Real-Time PCR System (Applied Biosystems) in duplicate for each sample.

For microRNA quantification, a TaqMan microRNA assay was used. 10 ng of total RNA were retro-transcribed in 20 μl total volume reaction containing 3 μl of 5× miRNA specific primers (RT 2300 hsa-miR-200c or RNU48 endogenous control; Applied Biosystems), 19 μl of 20 U/μl RNase inhibitor, 0.15 μl of 100 mM dNTPs and 1 μl of 50 U/μl Multiscribe Reverse Retrotranscriptase (Applied Biosystems). The reverse transcription conditions were 16°C for 30 min, 42°C for 30 min and 85°C for 5 min. 0.5 ng of the specific cDNA obtained was amplified in 15 μl total volume reaction containing 10 μl of TaqMan Universal Master Mix II no UNG (Applied Biosystems), 1 μl of specific primers and probes (TM230 miR-200c and 00106 miR-RNU48; Applied Biosystems). The PCR reaction was performed in duplicate for each sample as follows: 95°C for 10 min, 40 cycles at 95°C for 15 s and 60°C for 1 min. The relative levels of the different transcripts, expressed as $2^{-\Delta\Delta Ct}$, are represented as fold change with respect to control samples considered equal to 1.

Protein extraction, western blotting and immunoprecipitation
At the indicated time points, primary tubular cell cultures were lysed as described previously (Bianchi et al., 2013). 30 μg, or 60 μg when specified, of protein lysates quantified with a BCA microassay (Sigma-Aldrich) were separated on NuPage 4–12% gels (Invitrogen) and submitted to western blotting (Cifola et al., 2011) with the indicated antibodies (Table S1). For immunoprecipitation, cell lysates were prepared with RIPA buffer (50 mM Tris-HCl pH 7.4, 150 mM NaCl, 0.1% SDS, 0.5% sodium deoxicholate and 1% Nonidet P-40), containing a cocktail of protease and phosphatase inhibitors (Sigma-Aldrich). 2 mg of soluble proteins were subjected to immunoprecipitation using anti-Arg antibody and an Immunoprecipitation Starter Pack (GE Healthcare Bio-Science AB, Upsala), following the manufacturer's protocol. After immunoprecipitation the proteins, separated on NuPage 4–12% gels, were blotted and hybridized with anti-phosphotyrosine, anti-Arg and anti-ubiquitin antibodies (Table S1). Densitometric analysis of specific bands was performed by Image Scan Scanner with ImageJ software, and, for quantification, the specific band intensities were normalized to the corresponding β-actin, Smad2/3, Arg or p190RhoGAP band intensities when specified.

Wound healing assay
Monolayers of tubular cells, cultured in control and high-glucose medium on 6-well plates, were scratched with a pipette tip and photographed with a digital camera mounted on an inverted microscope Olympus (100× magnification). Matched pair-marked wound regions were photographed again after 8 h. Initial and final wound width was measured with ImageJ software. Three different measures in two different wells per sample were taken and expressed as mean±s.d. Wound recovery, calculated as difference between mean initial and final wound width, was used as a migration index.

Secreted TGF-β1 quantification by ELISA
Quantification of secreted TGF-β1 in tubular cell culture medium was performed with a Human TGF-β1 Platinum ELISA kit (BMS249/4, Bioscience) according to the manufacturer's instructions. Absorbance at 450 nm was measured using an automated microplate reader (Victor Wolla C1420, Perkin Elmer, Woltham, MA). Concentration values (pg/ml) were normalized to the cell protein concentration.

NIH3T3 growth curve
The NIH3T3 fibroblast cell line, cultured in high-glucose DMEM supplemented with 5% FBS (fibroblast medium), was serum-starved in DMEM for 24 h and then cultured in conditioned medium obtained from primary tubular cultures grown for 96 h in control medium, in high-glucose medium or in high-glucose medium plus Imatinib. NIH3T3 fibroblasts were also cultured in high-glucose conditioned medium or high-glucose conditioned medium plus Imatinib with the addition of 0.3 μM of the TGF-β receptor inhibitor SB431542 (Selleckchem, Houston, TX). The cell count, after 3, 24 and 48 h of treatment, was performed using Trypan Blue solution 0.4% (Sigma-Aldrich) with Thoma chamber. After 3 or 48 h of treatment with the different media, NIH3T3 cells were lysed as described above.

Intracellular ROS quantification
Cells were incubated with 10 μM DCF-DA (Sigma) for 40 min at 37°C in the dark. Fluorescent oxidized DCF in cell homogenate obtained by brief

sonication was measured at an excitation wavelength of 480 nm and an emission wavelength of 525 nm in dark 96-well plates using an automated microplate reader (Victor Wolla C1420). Mean relative fluorescence (RFU) was normalized to the cell protein concentration.

Arg and N-cadherin siRNA transfection

Subconfluent primary tubular cell cultures were transfected with ON-TARGETplus SMART pool Human ABL2 siRNA L-003101, ON-TARGETplus Control Pool siRNA D-001810-10-05 (Thermo Scientific Dharmacon, Lafayette, CO), or with human N-cadherin siRNA D-00101-0005 (Riboxx Life Sciences, Germany) using Interferin siRNA transfection reagent (Polyplus transfection; Thermo Scientific) according to the manufacturer's instructions, and then cultured for 96 h in high-glucose or control medium.

Proteasome activity assay

Proteasome peptidase activity was assayed on 30 µg of protein lysate using a 20S Proteasome Activity Assay kit (Chemicon APT280; Millipore, Watford, UK) and following the manufacturer's instructions. The fluorescent signal of AMC released from Suc-LLVT-AMC substrate after digestion was measured with a fluorescence spectrometer (Victor Wolla C1420), at an excitation wavelength of 380 nm and an emission wavelength of 460 nm, and expressed as the mean±s.d. relative fluorescence units (RFU).

Detection of GTP-bound RhoA

Active GTP-bound RhoA was measured in cell lysates using a RhoA activation G-LISA kit (BK124; Cytoskeleton Inc., Denver, CO) following the manufacturer's instruction. Briefly, cell lysates of control and high-glucose-treated samples were quantified for protein content, diluted to 0.5 mg/ml with lysis buffer and loaded in equal amounts onto a G-LISA plate for analysis. Absorbance values at 490 nm, measured using an automated microplate reader (Victor Wolla C1420) and corresponding to GTP-bound RhoA amount, were expressed as fold change with respect to control samples.

Statistical analysis

All molecular and functional effects of different cellular treatments were evaluated and/or quantified by two different operators blinded to experimental treatment. Data were analyzed using a Student's t-test to evaluate differences between two groups. Where differences between multiple groups were analyzed, one-way ANOVA followed by post-hoc Bonferroni's test was used. Values of $P<0.05$ were considered statistically significant. Unless otherwise stated, all data presented are expressed as mean±s.d. of at least three independent experiments.

Author contributions
B.T., C.B., and R.A.P. designed the research; B.T., C.M., V.D.S., L.I., S.D.M. and S. B. performed the experiments; G.B., R.B. and G.S. provided, processed and analyzed renal tissues; B.T., C.B. and R.A.P. wrote the paper. R.A.P. was responsible for the final decision to publish.

Supplementary information
Supplementary information available online at
http://jcs.biologists.org/lookup/suppl/doi:10.1242/jcs.183640/-/DC1

References

Bianchi, C., Torsello, B., Angeloni, V., Bombelli, S., Soldi, M., Invernizzi, L., Brambilla, P. and Perego, R. (2008). Eight full-length Abelson related gene (Arg) isoforms are constitutively expressed in caki-1 cell line and cell distribution of two isoforms has been analyzed after transfection. *J. Cell. Biochem.* **105**, 1219-1227.

Bianchi, C., Bombelli, S., Raimondo, F., Torsello, B., Angeloni, V., Ferrero, S., Di Stefano, V., Chinello, C., Cifola, I., Invernizzi, L. et al. (2010). Primary cell cultures from human renal cortex and renal-cell carcinoma evidence a differential expression of two spliced isoforms of Annexin A3. *Am. J. Pathol.* **176**, 1660-1670.

Bianchi, C., Torsello, B., Di Stefano, V., Zipeto, M. A., Facchetti, R., Bombelli, S. and Perego, R. A. (2013). One isoform of Arg/Abl2 tyrosine kinase is nuclear and the other seven cytosolic isoforms differently modulate cell morphology, motility and the cytoskeleton. *Exp. Cell Res.* **319**, 2091-2102.

Bombelli, S., Zipeto, M. A., Torsello, B., Bovo, G., Di Stefano, V., Bugarin, C., Zordan, P., Viganò, P., Cattoretti, G., Strada, G. et al. (2013). PKHhigh cells within clonal human nephrospheres provide a purified adult renal stem cell population. *Stem Cell Res.* **11**, 1163-1177.

Buchdunger, E., Zimmermann, J., Mett, H., Meyer, T., Müller, M., Druker, B. J. and Lydon, N. B. (1996). Inhibition of the Abl protein-tyrosine kinase in vitro and in vivo by a 2-phenylaminopyrimidine derivative. *Cancer Res.* **56**, 100-104.

Burns, W. C., Twigg, S. M., Forbes, J. M., Pete, J., Tikellis, C., Thallas-Bonke, V., Thomas, M. C., Cooper, M. E. and Kantharidis, P. (2006). Connective tissue growth factor plays an important role in advanced glycation end product-induced tubular epithelial-to-mesenchymal transition: implications for diabetic renal disease. *J. Am. Soc. Nephrol.* **17**, 2484-2494.

Cao, C., Li, Y., Leng, Y., Li, P., Ma, Q. and Kufe, D. (2005). Ubiquitination and degradation of the Arg tyrosine kinase is regulated by oxidative stress. *Oncogene* **24**, 2433-2440.

Carew, R. M., Wang, B. and Kantharidis, P. (2012). The role of EMT in renal fibrosis. *Cell Tissue Res.* **347**, 103-116.

Cifola, I., Bianchi, C., Mangano, E., Bombelli, S., Frascati, F., Fasoli, E., Ferrero, S., Di Stefano, V., Zipeto, M. A., Magni, F. et al. (2011). Renal cell carcinoma primary cultures maintain genomic and phenotypic profile of parental tumor tissues. *BMC Cancer* **11**, 244.

Daniels, C. E., Wilkes, M. C., Edens, M., Kottom, T. J., Murphy, S. J., Limper, A. H. and Leof, E. B. (2004). Imatinib mesylate inhibits the profibrogenic activity of TGF-beta and prevents bleomycin-mediated lung fibrosis. *J. Clin. Invest.* **114**, 1308-1316.

de Boer, I. H., Rue, T. C., Hall, Y. N., Heagerty, P. J., Weiss, N. S. and Himmelfarb, J. (2011). Temporal trends in the prevalence of diabetic kidney disease in the United States. *JAMA* **305**, 2532-2539.

Dolman, M. E. M., van Dorenmalen, K. M., Pieters, E. H. E., Lacombe, M., Pato, J., Storm, G., Hennink, W. E. and Kok, R. J. (2012). Imatinib-ULS-lysozyme: a proximal tubular cell-targeted conjugate of imatinib for the treatment of renal diseases. *J. Control Release* **157**, 461-468.

Druker, B. J. and Lydon, N. B. (2000). Lessons learned from the development of an Abl tyrosine kinase inhibitor for chronic myelogenous leukemia. *J. Clin. Invest.* **105**, 3-7.

Elliott, P. J., Zollner, T. M. and Boehncke, W. H. (2003). Proteasome inhibition: a new anti-inflammatory strategy. *J. Mol. Med.* **81**, 235-245.

Fragiadaki, M., Witherden, A. S., Kaneko, T., Sonnylal, S., Pusey, C. D., Bou-Gharios, G. and Mason, R. M. (2011). Interstitial fibrosis is associated with increased COL1A2 transcription in AA-injured renal tubular epithelial cells in vivo. *Matrix Biol.* **30**, 396-403.

Fraser, D., Brunskill, N., Ito, T. and Phillips, A. (2003). Long-term exposure of proximal tubular epithelial cells to glucose induces transforming growth factor-beta 1 synthesis via an autocrine PDGF loop. *Am. J. Pathol.* **163**, 2565-2574.

Gilbert, R. E. and Cooper, M. E. (1999). The tubulointerstitium in progressive diabetic kidney disease: more than an aftermath of glomerular injury? *Kidney Int.* **56**, 1627-1637.

Gu, L., Gao, Q., Ni, L., Wang, M. and Shen, F. (2013). Fasudil inhibits epithelial-myofibroblast transdifferentiation of human renal tubular epithelial HK-2 cells induced by high glucose. *Chem. Pharm. Bull.* **61**, 688-694.

Hernández, S. E., Settleman, J. and Koleske, A. J. (2004). Adhesion-dependent regulation of p190RhoGAP in the developing brain by the Abl-related gene tyrosine kinase. *Curr. Biol.* **14**, 691-696.

Hertig, A., Aglicheau, D., Verine, J., Pallet, N., Touzot, M., Ancel, P.-Y., Mesnard, L., Brousse, N., Baugey, E., Glotz, D. et al. (2008). Early epithelial phenotypic changes predict graft fibrosis. *J. Am. Soc. Nephrol.* **19**, 1584-1591.

Hills, C. E. and Squires, P. E. (2011). The role of TGF-β and epithelial-to mesenchymal transition in diabetic nephropathy. *Cytokine Growth Factor Rev.* **22**, 131-139.

Hills, C. E., Siamantouras, E., Smith, S. W., Cockwell, P., Liu, K.-K. and Squires, P. E. (2012). TGFβ modulates cell-to-cell communication in early epithelial-to-mesenchymal transition. *Diabetologia* **55**, 812-824.

Humphreys, B. D., Lin, S.-L., Kobayashi, A., Hudson, T. E., Nowlin, B. T., Bonventre, J. V., Valerius, M. T., McMahon, A. P. and Duffield, J. S. (2010). Fate tracing reveals the pericyte and not epithelial origin of myofibroblasts in kidney fibrosis. *Am. J. Pathol.* **176**, 85-97.

Iwano, M., Plieth, D., Danoff, T. M., Xue, C., Okada, H. and Neilson, E. G. (2002). Evidence that fibroblasts derive from epithelium during tissue fibrosis. *J. Clin. Invest.* **110**, 341-350.

Keller, C., Kroening, S., Zuehlke, J., Kunath, F., Krueger, B. and Goppelt-Struebe, M. (2012). Distinct mesenchymal alterations in N-cadherin and E-cadherin positive primary renal epithelial cells. *PLoS ONE* **7**, e43584.

Koesters, R., Kaissling, B., LeHir, M., Picard, N., Theilig, F., Gebhardt, R., Glick, A. B., Hähnel, B., Hosser, H., Gröne, H.-J. et al. (2010). Tubular overexpression of transforming growth factor-β1 induces autophagy and fibrosis but not mesenchymal transition of renal epithelial cells. *Am. J. Pathol.* **177**, 632-643.

Lassila, M., Jandeleit-Dahm, K., Seah, K. K., Smith, C. M., Calkin, A. C., Allen, T. J. and Cooper, M. E. (2005). Imatinib attenuates diabetic nephropathy in apolipoprotein E-knockout mice. *J. Am. Soc. Nephrol.* **16**, 363-373.

Lee, Y. J. and Han, H. J. (2010). Troglitazone ameliorates high glucose-induced EMT and dysfunction of SGLTs through PI3K/Akt, GSK-3β, Snail1, and β-catenin in renal proximal tubule cells. *Am. J. Physiol. Renal Physiol.* **298**, F1263-F1275.

Lee, J. H., Kim, J. H., Kim, J. S., Chang, J. W., Kim, S. B., Park, J. S. and Lee, S. K. (2013). AMP-activated protein kinase inhibits TGF-β-, angiotensin II-, aldosterone-, high glucose-, and albumin-induced epithelial-mesenchymal transition. *Am. J. Physiol. Renal Physiol.* **304**, F686-F697.

Li, D., Dong, Q., Tao, Q., Gu, J., Cui, Y., Jiang, X., Yuan, J., Li, W., Xu, R., Jin, Y. et al. (2015). c-Abl regulates proteasome abundance by controlling the ubiquitin-proteasomal degradation of PSMA7 subunit. *Cell Rep.* **10**, 484-496.

Lin, S.-L., Kisseleva, T., Brenner, D. A. and Duffield, J. S. (2008). Pericytes and perivascular fibroblasts are the primary source of collagen-producing cells in obstructive fibrosis of the kidney. *Am. J. Pathol.* **173**, 1617-1627.

Liu, Y. (2004). Epithelial to mesenchymal transition in renal fibrogenesis: pathologic significance, molecular mechanism, and therapeutic intervention. *J. Am. Soc. Nephrol.* **15**, 1-12.

Liu, X., Huang, W., Li, C., Li, P., Yuan, J., Li, X., Qiu, X.-B., Ma, Q. and Cao, C. (2006). Interaction between c-Abl and Arg tyrosine kinases and proteasome subunit PSMA7 regulates proteasome degradation. *Mol. Cell* **22**, 317-327.

Luo, Z.-F., Qi, W., Feng, B., Mu, J., Zeng, W., Guo, Y.-H., Pang, Q., Ye, Z.-L., Liu, L. and Yuan, F.-H. (2011). Prevention of diabetic nephropathy in rats through enhanced renal antioxidative capacity by inhibition of the proteasome. *Life Sci.* **88**, 512-520.

Mutlu, G. M., Budinger, G. R. S., Wu, M., Lam, A. P., Zirk, A., Rivera, S., Urich, D., Chiarella, S. E., Go, L. H. T., Ghosh, A. K. et al. (2012). Proteasomal inhibition after injury prevents fibrosis by modulating TGF-β1 signalling. *Thorax* **67**, 139-146.

Okuda, K., Weisberg, E., Gilliland, D. G. and Griffin, J. D. (2001). ARG tyrosine kinase activity is inhibited by STI571. *Blood* **97**, 2440-2448.

Peacock, J. G., Miller, A. L., Bradley, W. D., Rodriguez, O. C., Webb, D. J. and Koleske, A. J. (2007). The Abl-related gene tyrosine kinase acts through p190RhoGAP to inhibit actomyosin contractility and regulate focal adhesion dynamics upon adhesion to fibronectin. *Mol. Biol. Cell* **18**, 3860-3872.

Perego, R. A., Bianchi, C., Corizzato, M., Eroini, B., Torsello, B., Valsecchi, C., Di Fonzo, A., Cordani, N., Favini, P., Ferrero, S. et al. (2005). Primary cell cultures arising from normal kidney and renal cell carcinoma retain the proteomic profile of corresponding tissues. *J. Proteome Res.* **4**, 1503-1510.

Rastaldi, M. P., Ferrario, F., Giardino, L., Dell'Antonio, G., Grillo, C., Grillo, P., Strutz, F., Müller, G. A., Colasanti, G. and D'Amico, G. (2002). Epithelial-mesenchymal transition of tubular epithelial cells in human renal biopsies. *Kidney Int.* **62**, 137-146.

Rocco, M. V., Chen, Y., Goldfarb, S. and Ziyadeh, F. N. (1992). Elevated glucose stimulates TGF-beta gene expression and bioactivity in proximal tubule. *Kidney Int.* **41**, 107-114.

Shen, N., Lin, H., Wu, T., Wang, D., Wang, W., Xie, H., Zhang, J. and Feng, Z. (2013). Inhibition of TGF-β1-receptor posttranslational core fucosylation attenuates rat renal interstitial fibrosis. *Kidney Int.* **84**, 64-77.

Tashiro, K., Tamada, S., Kuwabara, N., Komiya, T., Takekida, K., Asai, T., Iwao, H., Sugimura, K., Matsumura, Y., Takaoka, M. et al. (2003). Attenuation of renal fibrosis by proteasome inhibition in rat obstructive nephropathy: possible role of nuclear factor kappaB. *Int. J. Mol. Med.* **12**, 587-592.

Wallace, E. and Gewin, L. (2013). Imatinib: novel treatment of immune-mediated kidney injury. *J. Am. Soc. Nephrol.* **24**, 694-701.

Wang, S., Wilkes, M. C., Leof, E. B. and Hirschberg, R. (2005). Imatinib mesylate blocks a non-Smad TGF-beta pathway and reduces renal fibrogenesis in vivo. *FASEB J.* **19**, 1-11.

Wang, S., Wilkes, M. C., Leof, E. B. and Hirschberg, R. (2010). Noncanonical TGF-beta pathways, mTORC1 and Abl, in renal interstitial fibrogenesis. *Am. J. Physiol. Renal Physiol.* **298**, F142-F149.

Zoja, C., Corna, D., Rottoli, D., Zanchi, C., Abbate, M. and Remuzzi, G. (2006). Imatinib ameliorates renal disease and survival in murine lupus autoimmune disease. *Kidney Int.* **70**, 97-103.
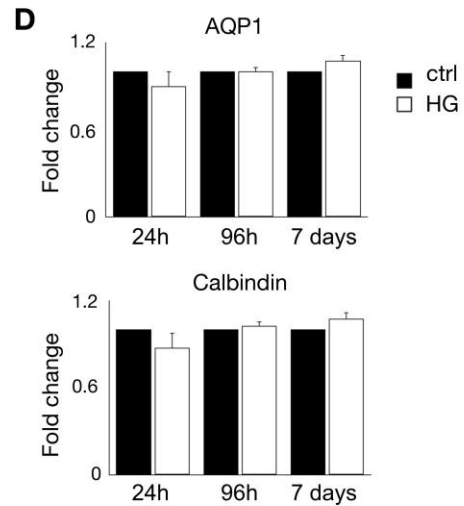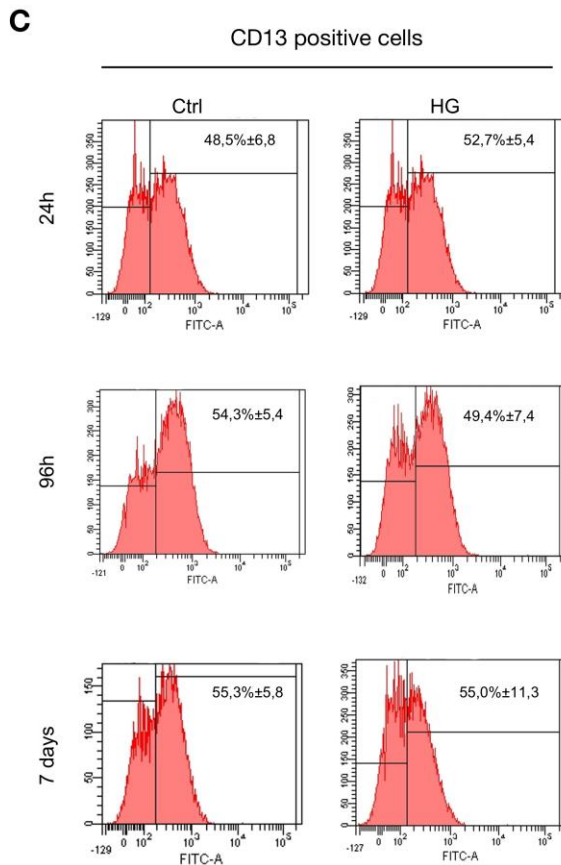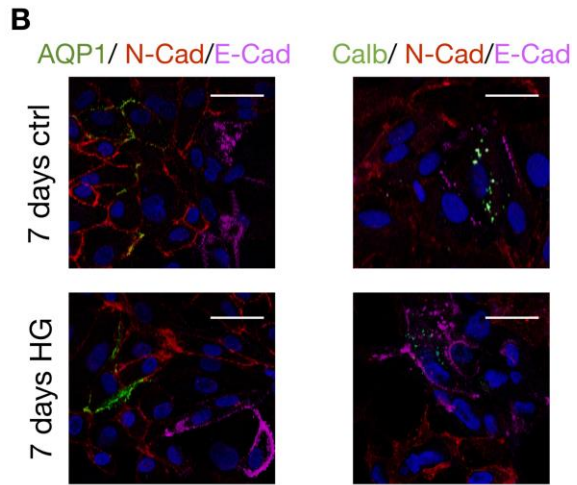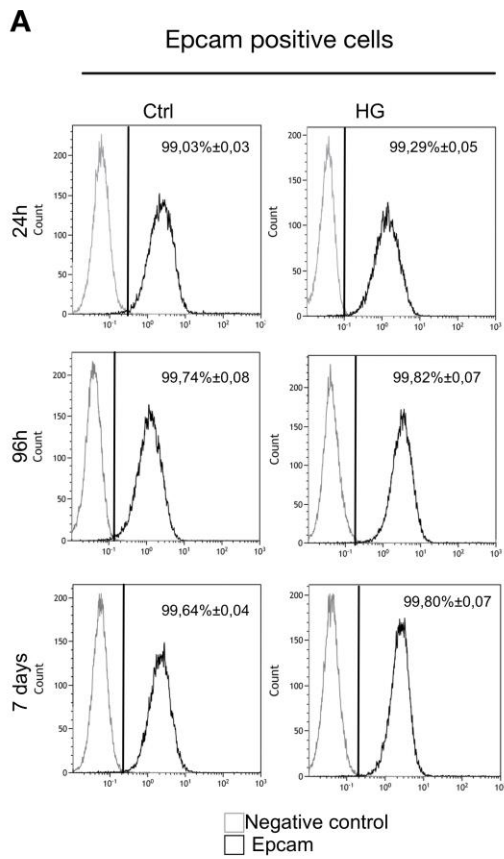
A

Epcam positive cells

Ctrl HG

24h

99,03%±0,03

99,29%±0,05

96h

99,74%±0,08

99,82%±0,07

7 days

99,64%±0,04

99,80%±0,07

☐ Negative control
☐ Epcam

B

AQP1/ N-Cad/E-Cad   Calb/ N-Cad/E-Cad

7 days ctrl

7 days HG

C

CD13 positive cells

Ctrl HG

24h

48,5%±6,8

52,7%±5,4

96h

54,3%±5,4

49,4%±7,4

7 days

55,3%±5,8

55,0%±11,3

D

AQP1

Calbindin

■ ctrl
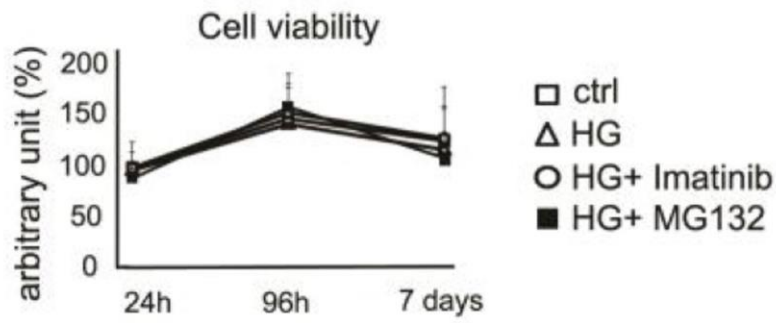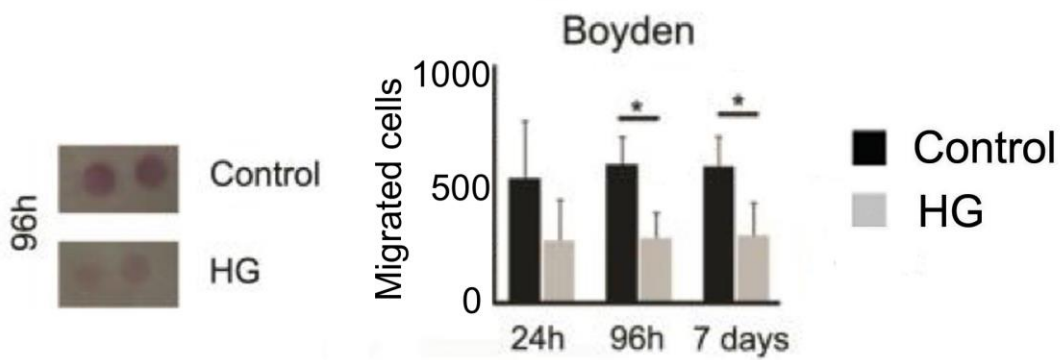☐ HG

24h   96h   7 days

Fold change

Fig. S1. (A and C) The percentage of cells positive for the epithelial marker Epcam and proximal tubular marker CD13 did not changed in HG treated primary cultures. Primary tubular cells cultured in control or HG media for 24, 96 hours or 7 days were stained with (A) anti-Epcam and corresponding secondary antibodies or with secondary antibodies alone (negative control), or with (C) anti-CD13 FITC antibody. FACS analysis was performed with MOFLO ASTRIOS and analyzed by Kaluza software (Beckman Coulter). The acquisition process was stopped when 20,000 events were collected in the population gate. Percentage of (A) Epcam-positive or (C) CD13-positive cells was reported as mean±s.d. of three independent experiments. (B) Proximal tubular marker AQP1 was detected only in N-cadherin-positive cells and distal tubular marker calbindin only in E-cadherin-positive cells in both HG treated and control tubular cells. Representative confocal microscopy images of tubular cells cultured for 7 days in control and HG condition. Proximal (AQP1) and distal (calbindin) tubular markers in green, N-cadherin in red and E-cadherin in pink. DAPI counterstains the nuclei in blue. Bar, 10 μm. (D) The protein expression of proximal and distal tubular markers did not change in HG-treated primary cultures. The protein expression of proximal (AQP1) and distal (calbindin) tubular markers was evaluated by Western Blot in lysates of primary cell cultures grown at different time point in control (ctrl) and HG medium. The data normalized for β-actin expression were expressed as fold change respect to corresponding control samples (unpaired t-test, n=3, mean±s.d.).

A

Cell viability

□ ctrl
△ HG
○ HG+ Imatinib
■ HG+ MG132

B

Boyden

■ Control
☐ HG

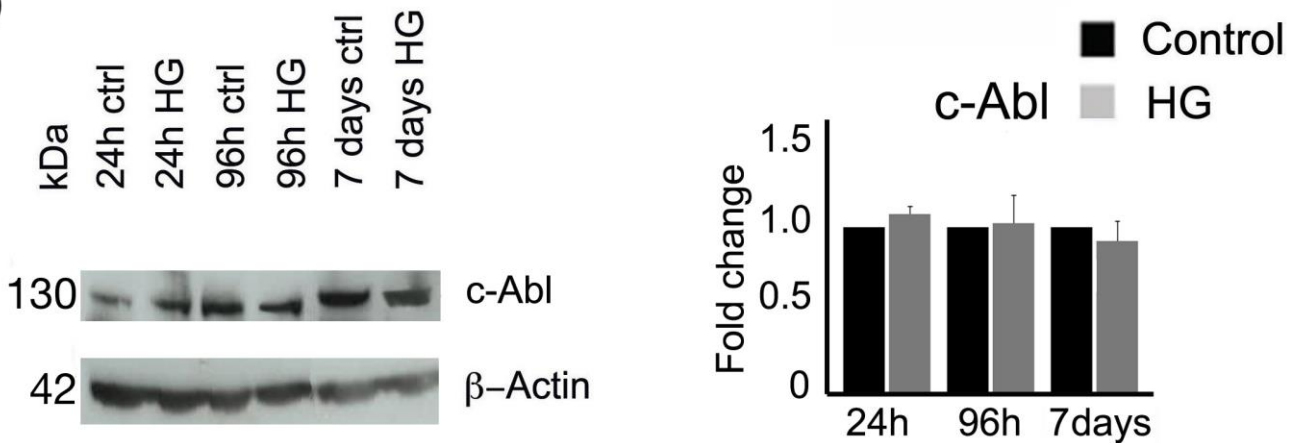**C**

D

■ Control
☐ HG

c-Abl

Fig. S2. (A) HG, Imatinib and MG132 treatment did not change cell viability of primary tubular cell cultures. Cell viability was measured by MTT assay (Sigma-Aldrich, St. Louis, MO) according to manufacturer's instructions. Absorbance at 550 nm was measured using an automated microplate reader (Bio-Rad 550, California, USA). Viability data after treatment at different time points with control (□ ctrl), high glucose (Δ HG), high glucose plus Imatinib (◯ HG+Imatinib) and high glucose plus MG132 (■HG+MG132) media, were expressed as percentage respect to cells treated for 24 hours with control media. No significant changes in cell viability were observed with the different treatments at any time points (one-way ANOVA with Bonferroni's test, *$p<0.05$, n=3, mean±s.d.). (B) HG treatment reduced cell motility in primary tubular cell cultures. Cell migration assay was carried out in Boyden chambers (containing 8 μm transwell membrane; Corning Costar Corp, Cambridge, MA) as described (Bianchi et al., 2013). 2 x 10^4 cells, grown in control or high glucose (HG) media for different time points, were seeded in the upper chamber and, after 6 hours at 37 °C, cells adherent to the lower membrane were fixed with cold methanol for 15 minutes, stained with Haematoxylin-Eosin solution (Sigma-Aldrich St. Louis, MO) and microphotographed. The migrated cells were counted with ImageJ software. Two membranes were analyzed for each sample. Representative pictures of stained membranes corresponding to cellular samples grown for 96 hours in control and HG media were reported. The graph reported the number of migrated cells expressed as mean±s.d. (unpaired t-test, *$p<0.05$, n=6). (C) PDGFR-β and c-Kit proteins were not expressed in our primary tubular cell cultures. Representative Western blot of 30 μg of protein lysates from primary cultures grown for 96 hours in control (ctrl) and HG media. β-Actin protein band was used as loading control. LX-2: LX-2 human fibroblast cell line lysate used as PDGFR-β positive control. TF-1: TF-1 erythroleukemia cell line lysate used as c-kit positive control. (D) c-Abl expression did not change in primary tubular cell cultures grown in HG condition. Representative Western blot of 60 μg of protein lysates from primary cultures grown for different time points in control (ctrl) and HG media. The protein bands of c-Abl and of β-Actin were shown. The normalized c-Abl band intensities were expressed as fold change respect to corresponding control samples. The bar graphs indicated the mean±s.d. (unpaired t-test, n=3).
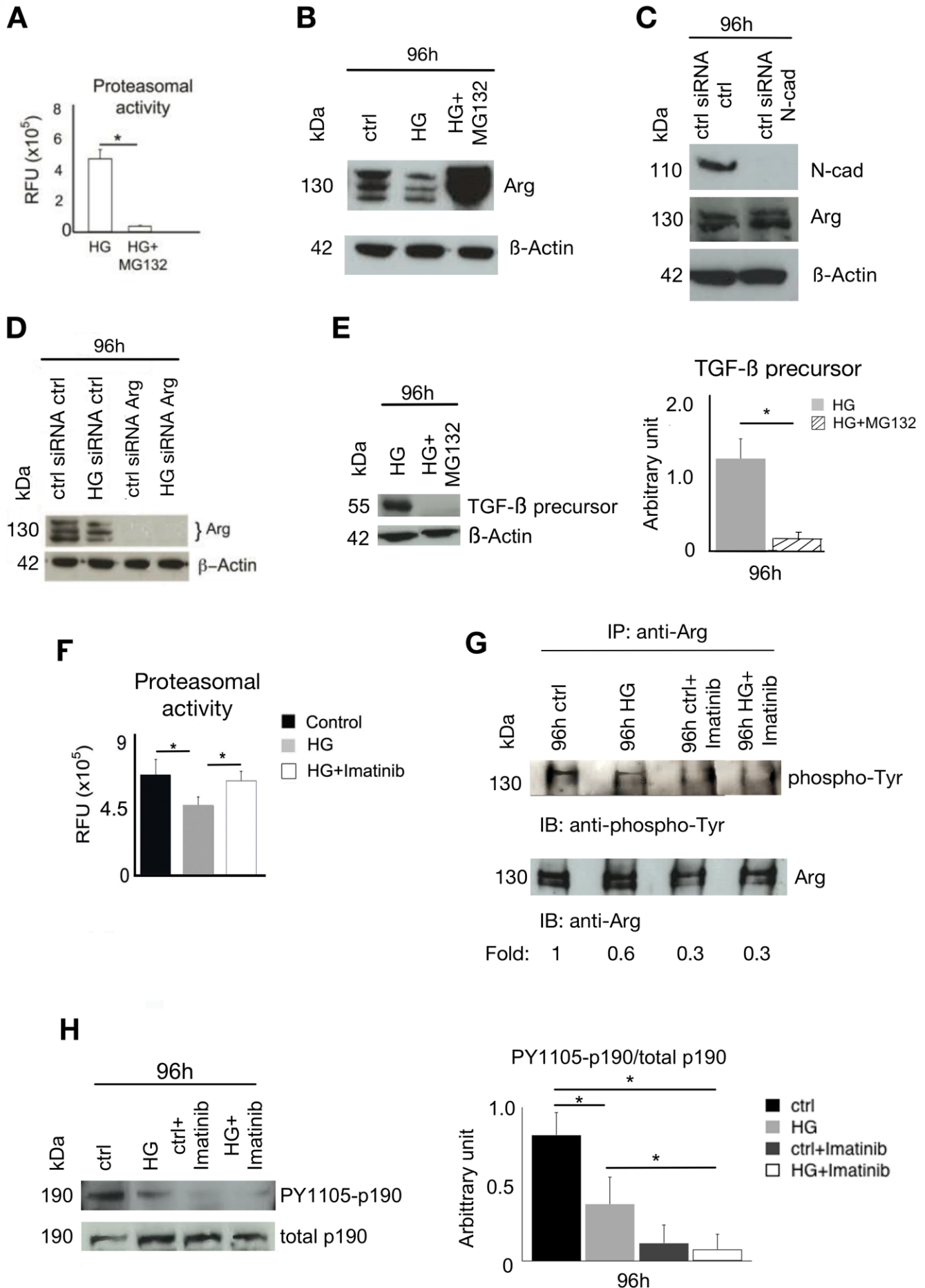
Fig. S3. (A, B and E) Proteasome activity inhibition by MG132 counteracted Arg decrement and induced TGF-β downregulation in HG treated tubular cells. Primary cultures grown for 96 hours in control (ctrl), high glucose (HG) or high glucose plus 10 μM MG132 (HG + MG132) media were assayed for (A) proteasome activity, by addition of Suc-LLVT-AMC substrate and quantification of released fluorescent signal, (B) Arg and (E) TGF-β expression, by Western blot. In (A) the data were expressed as mean relative fluorescent units (RFU) ±s.d.. In (B) Arg and β-Actin protein bands were shown. In (E) the protein bands of TGF-β precursor and of β-Actin were shown, and the normalized TGF-β band intensities were expressed in the graph as mean±s.d. (unpaired t-test, *p<0.05, n=3). (C) N-cadherin knockdown by siRNA did not affect Arg protein level in tubular cells grown in control medium. Representative western blot of protein lysates from primary cultures grown for 96 hours in control medium plus control siRNA (ctrl siRNA ctrl) or plus N-cadherin specific siRNA (ctrl siRNA N-cad) showing N-cadherin, Arg and β-Actin protein bands. (D) Validation of Arg knockdown by siRNA. Representative Western blot of protein lysates from primary cultures grown for 96 hours in control medium plus control siRNA (ctrl siRNA ctrl), high glucose medium plus control siRNA (HG siRNA ctrl), control medium plus Arg specific siRNA (ctrl siRNA Arg) or high glucose medium plus Arg specific siRNA (HG siRNA Arg), showing Arg and β-Actin protein bands. After specific silencing, Arg protein bands were almost undetectable. (F) High glucose (HG) but not HG plus Imatinib treatment induced proteasome activity downregulation in tubular cells. Proteasome activity was assayed in protein lysates of primary cultures grown for 96 hours in control, HG or HG plus Imatinib (HG+Imatinib) and expressed as mean relative fluorescent units (RFU) ±s.d. (one-way ANOVA with Bonferroni's test, *p<0.05, n=3) (G-H) Arg tyrosine kinase activity decreased in HG treated tubular cells and further decreased in presence of Imatinib. Cellular protein lysates of primary cultures grown for 96 hours in control (ctrl) medium, in medium containing HG (HG), Imatinib (ctrl+Imatinib) or HG plus Imatinib (HG+Imatinib) were (G) immunoprecipitated with anti-Arg antibodies, blotted and hybridized with anti-phosphotyrosine and anti-Arg antibodies, or (H) analyzed by Western blot. In (G) the tyrosine-phosphorylated Arg band intensities normalized with the corresponding total Arg band were expressed as fold change (Fold) respect to control sample. In (H) the bands of site-specific (Y1105) phosphorylated p190RhoGAP (PY1105-p190) and total p190RhoGAP (total p190) proteins were shown, and the PY1105-p190 band intensities normalized with the corresponding total p190 band were expressed in the graph as mean±s.d. (one-way ANOVA with Bonferroni's test, *p<0.05, n=3).

Table S1. Characteristics of primary and secondary antibodies used in the study

Antibody	Clone	Company	Source	Dilution I.F./ FACS	Dilution I.P.	Dilution W.B.
anti- Pancytokeratin		Dako, Glostrup, DK	Mouse	1:200		
anti-Epcam	HEA-125	GeneTex, Irvine, CA	Mouse	1:1000/1:20		
anti-E-Cadherin	36	Becton Dickinson, San Josè, California	Mouse	1:50		1:1000
anti-E-Cadherin -APC	67A4	Biolegend, San Diego, CA	Mouse	1:20		
anti-N-Cadherin	ab76057	Abcam, Cambridge, UK	Rabbit	1:50		
anti-N-Cadherin	32/N	Becton Dickinson, San Josè, California	Mouse			1:1000
anti-AQP1	B-11	Santa Cruz Biotechnology Heidelberg, Germany	Mouse	1:50		1:200
anti-Calbindin	CB-955	Sigma-Aldrich, St. Louis, MO	Mouse	1:100		1:1000
anti-CD13 FITC	WM15	Abcam, Cambridge, UK	Mouse	1:25/1:10		
anti-Vimentin		Dako, Glostrup, DK	Mouse			1:1000
anti-Arg		Millipore, Upstate, Lake Placid, NY	Rabbit		1:5	1:400
anti-α-sma		Dako, Glostrup, DK	Rabbit			1:1000
anti-ZO-1		Abcam, Cambridge, UK	Rabbit			1:500
anti-TGF-β		Cell Signaling, Boston, MA	Rabbit			1:1000
anti-Phospho-Smad2 (Ser465/467)		Cell Signaling, Boston, MA	Rabbit			1:1000
anti-Smad 2/3		Cell Signaling, Boston, MA	Rabbit			1:1000
anti-c-Abl		Santa Cruz Biotechnology Heidelberg, Germany	Rabbit			1:1000
anti-Phospho tyrosine	4G10	Millipore, Upstate, Lake Placid, NY	Mouse			1:1000
anti-PhosphoY1105 p190		Abcam, Cambridge, UK	Rabbit			1:100
anti-p190		Becton Dickinson, San Josè, California	Mouse			1:250
anti-PDGFR-β		Santa Cruz Biotechnology Heidelberg, Germany	Rabbit			1:1000
anti-c-Kit		Dako, Glostrup, DK	Rabbit			1:1000
anti-β-actin		Sigma-Aldrich, St. Louis, MO	Rabbit			1:1000
anti-Ubiquitin		Cell Signaling, Boston, MA	Rabbit			1:1000
anti-RhoA		Santa Cruz Biotechnology Heidelberg, Germany	Mouse			1:1000
Alexa 594 conjugated anti-rabbit IgG		Molecular Probes, Carlsberg, CA	Goat	1:100		
Alexa 488 conjugated anti-mouse IgG		Molecular Probes, Carlsberg, CA	Goat	1:100		

I.F. immunofluorescence; **I.P.** immunoprecipitation; **W.B.** Western blot.

Table S2. TaqMan gene expression assays used in the study

Gene name	Gene expression assay	Species	Company
N-Cadherin	Hs00362037_m1	Human	Applied Biosystem
E-Cadherin	Hs01023894_m1	Human	Applied Biosystem
S100A4	Hs00243202_m1	Human	Applied Biosystem
Col1a2	Hs00164099_m1	Human	Applied Biosystem
TGF-β1	Hs00998133_m1	Human	Applied Biosystem
GAPDH	Hs99998805_m1	Human	Applied Biosystem